

# Longitudinal Cutting of Pure and Doped Carbon Nanotubes to Form Graphitic Nanoribbons Using Metal Clusters as Nanoscalpels

Ana Laura Elías,<sup>†</sup> Andrés R. Botello-Méndez,<sup>†</sup> David Meneses-Rodríguez,<sup>†</sup> Viviana Jehová González,<sup>†</sup> Daniel Ramírez-González,<sup>†</sup> Lijie Ci,<sup>‡</sup> Emilio Muñoz-Sandoval,<sup>†</sup> Pulickel M. Ajayan,<sup>‡</sup> Humberto Terrones,<sup>†</sup> and Mauricio Terrones<sup>\*†</sup>

<sup>†</sup>Laboratory for Nanoscience and Nanotechnology Research (LINAN) and Advanced Materials Department, IPICYT, Camino a la Presa San José 2055, Col. Lomas 4a. sección, San Luis Potosí 78216, SLP, México, <sup>‡</sup>Department of Mechanical Engineering and Materials Science, Rice University, Houston, Texas 77005

**ABSTRACT** We report the use of transition metal nanoparticles (Ni or Co) to longitudinally cut open multiwalled carbon nanotubes in order to create graphitic nanoribbons. The process consists of catalytic hydrogenation of carbon, in which the metal particles cut  $sp^2$  hybridized carbon atoms along nanotubes that results in the liberation of hydrocarbon species. Observations reveal the presence of unzipped nanotubes that were cut by the nanoparticles. We also report the presence of partially open carbon nanotubes, which have been predicted to have novel magnetoresistance properties.<sup>1</sup> The nanoribbons produced are typically 15–40 nm wide and 100–500 nm long. This method offers an alternative approach for making graphene nanoribbons, compared to the chemical methods reported recently in the literature.

**KEYWORDS** Catalytic, hydrogenation, graphene, cutting, nitrogen-doped carbon nanotubes, carbon nanoribbons

The discovery of graphene and, consequently, graphene nanoribbons (GNRs) has set a new dimension for nanoscale carbon science.<sup>2,3</sup> These one atom thick materials exhibit outstanding and unusual properties that can potentially lead to numerous applications in electronics, sensors, composites, etc.<sup>3</sup> Even before the discovery of graphene, the properties of GNRs were thoroughly studied theoretically since they were an ideal system to understand the properties of single-walled nanotubes.<sup>5,6</sup> It turned out that these systems exhibit peculiar edge states that depend on their shape and their width. All GNRs less than ca. 10 nm wide could be semiconductors.<sup>7</sup> For larger widths, the shape of the edge largely determines the properties of the nanoribbon. Zigzag-shaped edges are metallic, whereas armchair-shaped edges could be semiconductive or semimetallic depending on their width.<sup>7</sup> Furthermore, zigzag nanoribbons become semimetallic under the effect of an electric field which could be applied externally, or with the adsorption of polar molecules at the edges.<sup>8,9</sup> In addition, the chemistry at nanoribbon edges is interesting and could be exploited in the fabrication of efficient sensor devices.<sup>10</sup> GNRs maintain the axial strength of carbon nanotubes but are considerably more flexible, with a bending stiffness 2 orders of magnitude less than that reported for carbon nanotubes.<sup>11</sup>

Now that graphene synthesis has become available, some of its predicted properties have been successfully verified experimentally.<sup>12</sup> Currently synthesis of graphene nanoribbons has been achieved using experimental methods with very low yield such as mechanical cleavage followed by lithography, etching, and chemical stripping.<sup>3,13,14</sup> Nevertheless, important efforts to achieve large scale synthesis of graphene nanoribbons have started to appear. Chemical vapor deposition (CVD) has been successfully carried out leading to bulk quantities of graphite nanoribbons which may be very useful for composites.<sup>15</sup> Another novel approach has been reported using carbon nanotubes (CNTs) as starting material and by unzipping them in a controlled way, nanoribbons of precise dimensions could result.<sup>16</sup> In this context, Tour and co-workers used a chemical attack based on sulfuric acid, potassium permanganate, and mild heating that opens up the tubes longitudinally.<sup>17</sup> Similarly, Cano-Márquez et al. have unzipped CNTs by the intercalation of lithium and ammonia.<sup>18</sup> However, in both cases the resulting graphite nanoribbons are wide (>10 nm) and could exhibit functionalized groups at the edges that affect their chemical and electronic properties. In addition, such methods have still little control on the structure of the edges of the nanoribbons produced. The group lead by Hongjie Dai has presented a multistep process in which arc-grown CNTs partially embedded in a polymer film are etched with an argon plasma.<sup>19</sup> Subsequently, the film is removed using solvent vapor followed by a heat treatment of the resulting

\* Corresponding author.

Received for review: 05/23/2009

Published on Web: 08/19/2009

nanoribbons to remove any residual polymer.<sup>19</sup> The key advantage of the latter technique is that very narrow graphene nanoribbons (<10 nm) could be produced, resulting in a sample of all semiconductor nanoribbons; however, this multistep method seems hardly scalable for the moment.

Brey and co-workers have recently proposed that carbon nanotubes could be the ultimate contacts for GNRs.<sup>1</sup> These authors found that GNRs from unzipped nanotubes theoretically behave as completely transparent contacts for the parent tubes, and vice versa. Their results demonstrate that partially unzipped carbon nanotubes constitute magnetoresistive devices, with large values of the magnetoresistance.<sup>1</sup>

Recently, Datta and co-workers,<sup>20</sup> and separately Ci and co-workers<sup>21,22</sup> demonstrated the controlled catalytic cutting of graphite by deposited metal nanoparticles. In this context, due to the catalytic action of the metal nanoparticle, carbon atoms in graphite diffuse on the nanoparticle at approximately 900 °C under an Ar–H atmosphere. Subsequently, the particle gets saturated and then reacts with H<sub>2</sub>, in a process that has been addressed in the literature as catalytic hydrogenation of carbon.<sup>23</sup> Depending on the particle size, the cutting could be driven along specific directions, forming either armchair or zigzag edges.<sup>21,22</sup>

In this work, we report, for the first time, the catalytic cutting of multiwalled carbon nanotubes (MWNTs) and nitrogen-doped multiwalled carbon nanotubes (CN<sub>x</sub>MWNTs) using either Co or Ni nanoparticles so as to unzip the tubes and form graphene sheets and GNRs. We have also obtained partially open nanotubes, which could exhibit novel magnetoresistive properties.<sup>1</sup> As previously reported for highly oriented pyrolytic graphite (HOPG),<sup>21,22</sup> we found that the cutting direction and depth are mostly determined by the particle size and the number of step edges where the nanoparticle nucleates. The experimental process could be understood as a reverse of CVD carbon nanofiber growth.

In our experiments, we used undoped MWNTs and CN<sub>x</sub>MWNTs synthesized by an aerosol pyrolysis system described elsewhere.<sup>24–26</sup> In both cases, the catalyst responsible for the growth was Fe, obtained from ferrocene (FeCp<sub>2</sub>). Toluene (C<sub>7</sub>H<sub>8</sub>) was used as carbon precursor for the synthesis of MWNTs,<sup>25</sup> and it was replaced by benzylamine (C<sub>7</sub>H<sub>9</sub>N) for the synthesis of CN<sub>x</sub>MWNTs.<sup>26</sup>

Either MWNTs or CN<sub>x</sub>MWNTs were added to a solution of 3% (wt) CoCl<sub>2</sub> in methanol CH<sub>3</sub>OH. This solution was dispersed ultrasonically with a high power sonication tip for 1 min, and ca. 30 μL were dropped on a clean Si wafer and allowed to dry to room temperature. The sample was then placed in a quartz tube, in the center of a tubular furnace. Subsequently, the substrate was heated to 500 °C for 1 h in order to allow a proper nucleation of the metal nanoparticles on the surface of the tubes. The catalytic hydrogenation of carbon was performed at 850 °C for 30 min. The carrier gas consisted of a mixture of Ar/H (90:10 by volume, respectively). Alternatively, a magnetron sputtering (modified INTERCOVAMEX-V3) was used to deposit the metal nanopar-

ticles on the carbon tubes. First, pristine CNTs were dispersed in methanol (100 μg/mL) with an ultrasonic bath, for 1 h. Fifty milliliters of this dispersion were allowed to evaporate at room temperature in a vial. In order to obtain a nanotube film, a Si wafer was located vertically against the wall of the vial, and a nanotube (either MWNTs or CN<sub>x</sub>MWNTs) film was formed due to capillary action during the evaporation of the solvent. A 2 nm film of Ni was subsequently deposited on the substrate using a pulsed dc magnetron sputtering during 5 s by an Ar plasma. The pressure of the chamber was 10<sup>-7</sup> Torr, the frequency corresponded to 50 kHz, and we used and input power of 60 W (ca. 0.17 A and 355 V). The sputtering deposition was carried out at 32 mTorr and at room temperature. The experimental conditions for the cutting with Ni nanoparticles were the same as those in the case of Co nanoparticles (850 °C for 30 min).

We carefully characterized the obtained samples using scanning electron microscopy (SEM), scanning transmission electron microscopy (STEM), transmission electron microscopy (TEM), and atomic force microscopy (AFM). Si wafers containing the nanotubes treated thermally were immersed in acetone and placed in an ultrasonic bath for 20 min; a few drops of this solution were placed on Cu grids for TEM and STEM observations. Both SEM and STEM were performed with an UHRSEM FEI XL30 SPEG (operating at 12 kV) and a DUAL BEAM FEI HELIOS 600 NANOLAB (operating at 2–5 kV). TEM was carried out with a HRTEM FEI TECNAI F30 STWIN G2, operated at 300 kV. AFM images were obtained using an AFM JEOL JSPM 5200.

Figure 1 shows SEM micrographs of the cutting process. Panels a, b, and d of Figure 1 exhibit metal nanoparticles nucleated on the surface of CN<sub>x</sub>MWNTs (see encircled areas). Chemically driven small nanoparticles traveled on the surface of the nanotubes creating mostly random cuts on the outer graphitic layers, via catalytic hydrogenation of the graphene sheets<sup>21–23</sup> (see Figure 1a). Larger metal nanoparticles (ca. 40 nm) traveled along the axis of some carbon nanotubes, performing deeper cuts (see Figure 1, panels b–d) that opened longitudinally MWNTs and CN<sub>x</sub>MWNTs, thus resulting in the creation of carbon nanoribbons and nanosheets (see Figures 1e and 2). In panels a–d of Figure 1, arrows guide the eye to point out the nanocutting of MWNTs and CN<sub>x</sub>MWNTs. Figure 2 depicts SEM and STEM images of the partially open CNTs, graphitic nanoribbons, and nanosheets produced in our experiments. Figure 2a exhibits a MWNT that is almost completely unzipped but still has short carbon nanotube segments at both ends, which constitutes a GNR with CNT leads. Its dimensions are approximately 20 nm wide and 500 nm long. After cutting N-doped MWNTs, different sized nanoribbons were produced (typically 15–40 nm wide and 100–500 nm long), as shown in Figure 2b. Occasionally, longer nanoribbons were observed during the electron microscopy characterization. Panels c and d of Figure 2 exhibit SEM and bright field (BF) STEM images obtained from the same twisted nanoribbon,

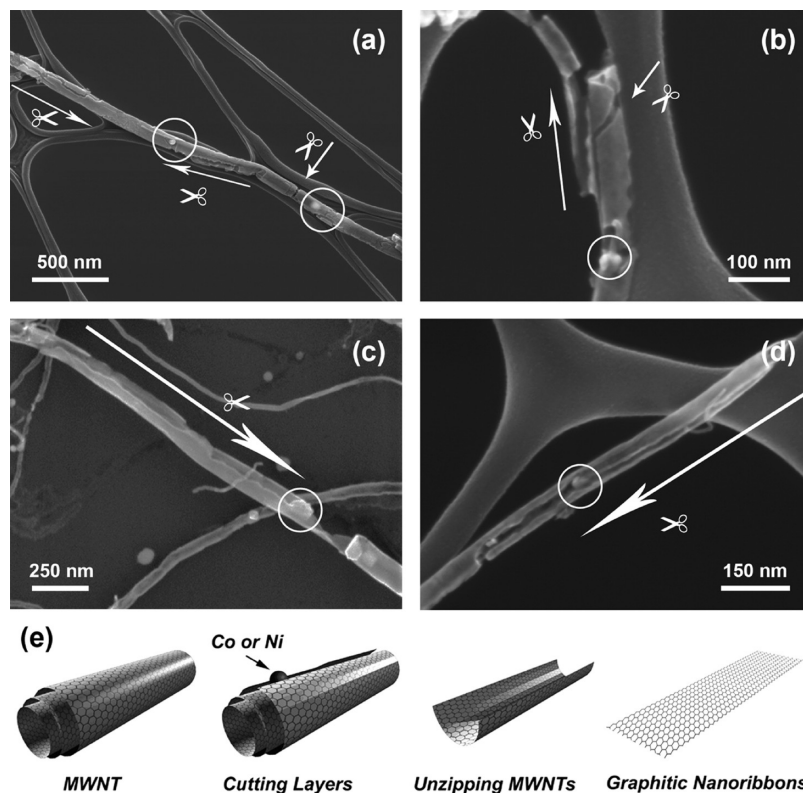


FIGURE 1. SEM micrographs of the prepared samples. ((a), (b), and (d)) SEM images of  $CN_x$ MWNTs cut with Ni nanoparticles. (c) SEM image of a MWNT on a Si substrate, with Co nanoparticles. Arrows guide the eye along the nanocutting and circles mark the presence of metal nanoparticles. (e) Schematic diagram representing different stages of cutting MWNTs along their axes with metal nanoparticles of Ni or Co. The scheme shows the unzipping process of an armchair MWNT so as to form a zigzag graphitic nanoribbon.

after  $CN_x$ MWNTs cutting experiments with Ni nanoparticles. We could also observe the presence of graphitic nanosheets in our samples. SEM and BF-STEM images of a large and irregular shaped nanosheet are shown in panels e and f of Figure 2.

Low-magnification TEM micrographs also reveal the cutting effect of catalyst nanoparticles on the surface of nanotubes. Figure 3a exhibits a short  $CN_x$ MWNT that has been unzipped by the effect of carbon hydrogenation. We have included a drawing model of the unzipped  $CN_x$ MWNT for a better understanding of the image. Sometimes, few layer graphene remains as the connection between the two ends of a carbon nanotube after the cutting process, as shown in panels b–d of Figure 1. In Figure 3c, arrows show the presence of the low contrast graphene layers. This type of hybrid structure has been theoretically predicted to be a magnetoresistive device.<sup>1</sup> We have included a high-resolution TEM image in order to show the good crystallinity of the nanotubes used in our experiments (see Figure 3d).

Si wafers covered with nanotubes and nanoribbons were characterized by AFM in order to get more accurate information on the shape and roughness of the unzipped nanostructures (see Figures 4 and 5). Figure 4a depicts an AFM topography image of two overlapped  $CN_x$ MWNTs and Figure 4b depicts a model of both nanotubes, in order to better understand the AFM image shown in Figure 4a. The

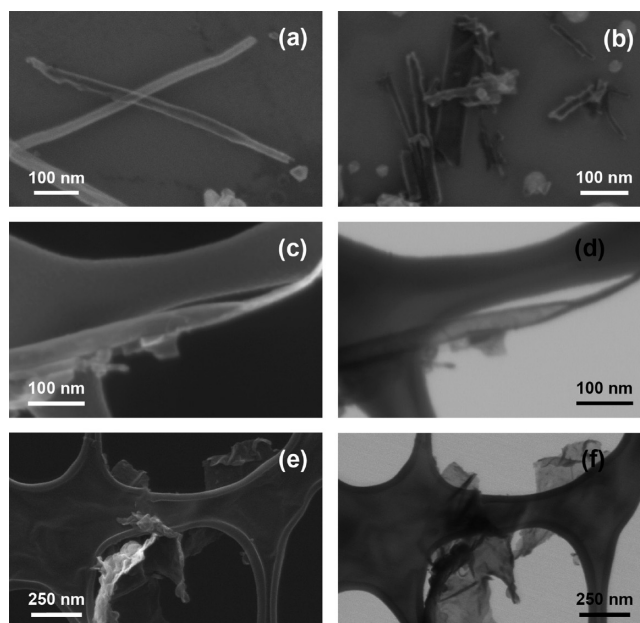


FIGURE 2. SEM and STEM micrographs of the produced graphitic nanoribbons and nanosheets. (a) SEM image of a MWNT almost completely unzipped. (b) SEM image of different sized nanoribbons, as a result of the cutting experiments on  $CN_x$ MWNTs with Ni sputtered nanoparticles. SEM (c) and bright field (BF) STEM (d) images of a twisted nanoribbon, from  $CN_x$ MWNT cutting experiments. SEM (e) and BF-STEM (f) images of a representative nanosheet obtained from an ultrasonic dispersed  $CN_x$ MWNT cut sample.

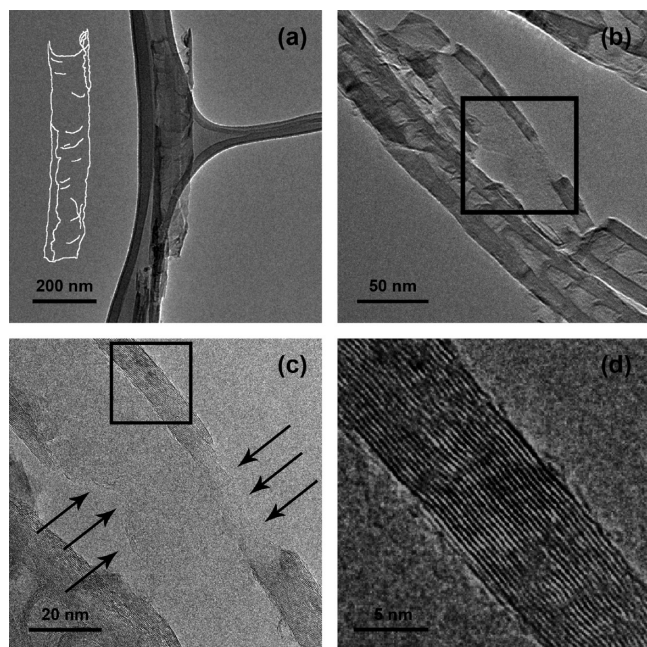


FIGURE 3. TEM micrographs of cut  $CN_x$ MWNTs. (a) and (b) Low-magnification images of  $CN_x$ MWNTs after the cutting process. (c) Higher magnification TEM micrograph that corresponds to the box in (b), where few layer graphene is bonding two parts of a  $CN_x$ MWNT, as the arrows point out. (d) High-resolution TEM image corresponding to the box in (c), which exhibits the (002) G planes present in carbon nanotubes.

nanotube on the top has been cut by a metal nanoparticle, and we were able to follow the nanoparticle track by analyzing the surface profile along different line scans

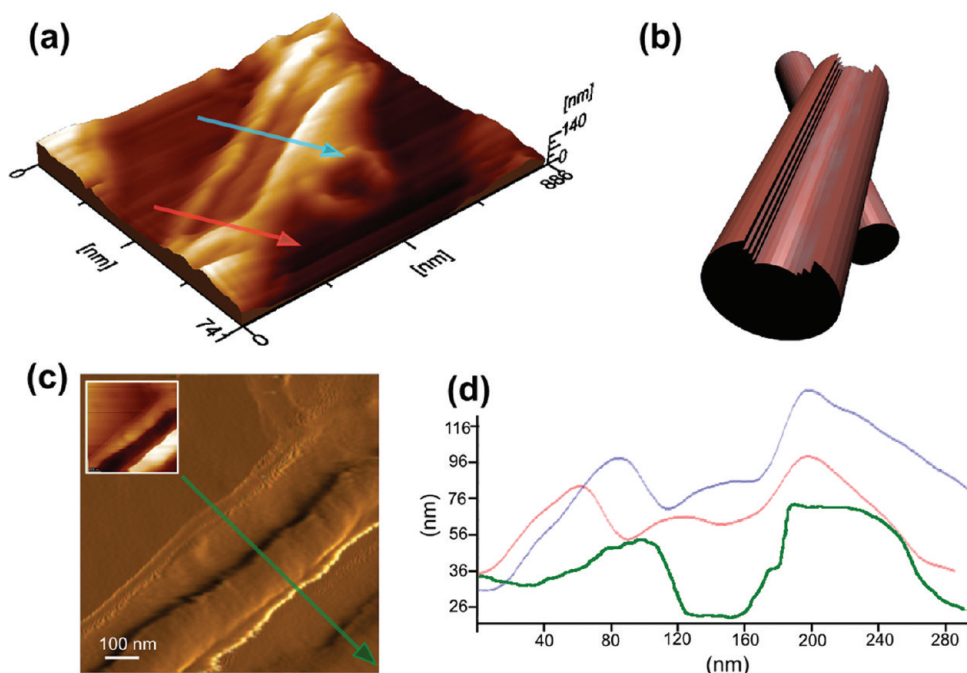


FIGURE 4. (a) AFM image of a  $CN_x$ MWNT cut along the axis. (b) Schematic model of the cut shown in (a). (c) rms roughness and topography (inset) AFM images of the detail of a nanotube cut along the axis. (d) Surface profiles along different lines of nanotube cuts shown in (a) and (c).

depicted by arrows (see Figure 4, panels a and d). Another example of  $CN_x$ MWNTs unzipped is exhibited in a root-mean-square (rms) roughness image (see Figure 4c). Here, the line profile (green) shows a deeper cut (see Figure 4, panels c and d). Figure 5a. exhibits an AFM image of a nanoribbon with its corresponding surface profile along five line scans (Figure 5b). In this case, a nanoparticle has cut a  $CN_x$ MWNT along the axis and transformed it into a GNR. We have included additional AFM images in the Supporting Information that show the difference in the AFM profiles of open tubes (always with a deep in the middle) when compared to standard tubes (with round profiles across the tube circumference).

During the experiment, carbon atoms are dissociated on the catalyst (Ni or Co nanoparticles) and, since the process takes place in an Ar-H atmosphere, dissociated carbon atoms further react with  $H_2$  to form methane ( $CH_4$ ).<sup>20-22</sup> The detailed characterization of our samples revealed that most of the tubes were either cut, partially open, or open along the axis. We also observed the presence of short graphitic nanoribbons by SEM. In addition, TEM and STEM studies revealed the presence of carbon nanosheets.

We would like to point out that the chirality of the nanotubes seems to play an important role during nanotube cutting. As it has been described in earlier reports for HOPG,<sup>21,22</sup> a catalyst particle is able to selectively cut graphene sheets along an armchair or zigzag atomic line. However, the chirality in the bulk CNT samples was not determined for individual tubes prior to the opening experiments. Previous reports<sup>27</sup> indicate that MWNTs exhibit

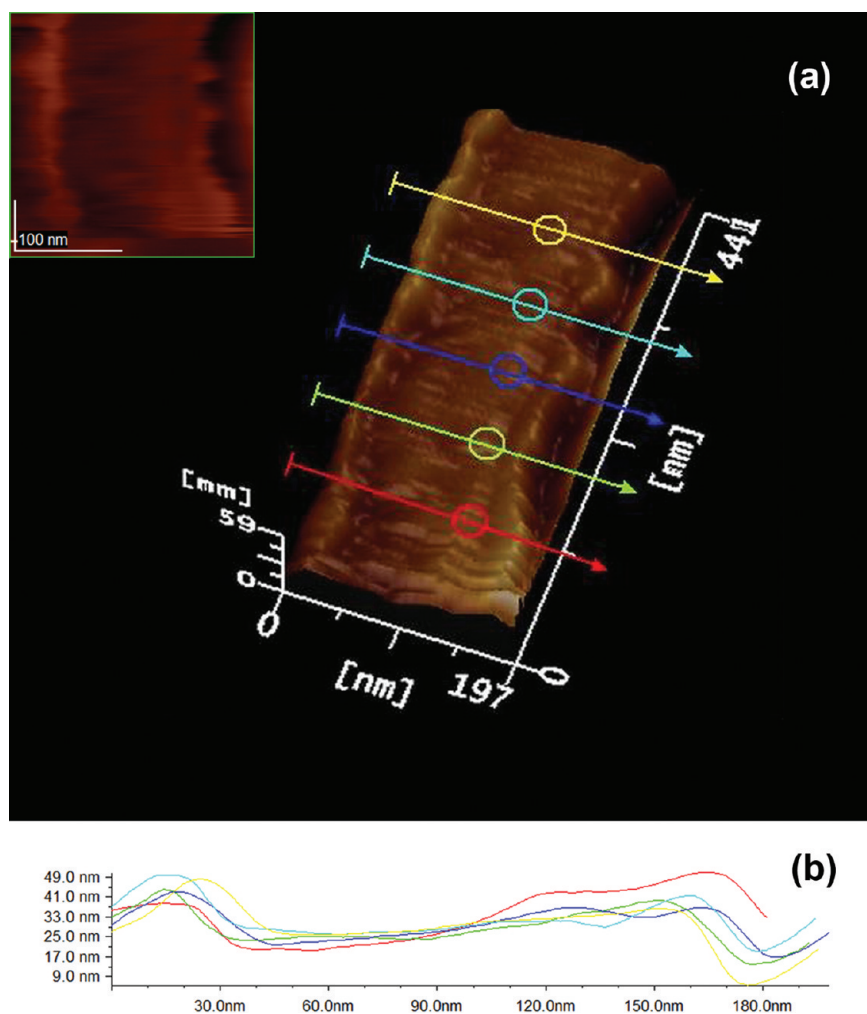


FIGURE 5. (a) AFM image of a GNR obtained from  $\text{CN}_x$ MWNT cutting experiments. The inset shows a higher magnification AFM image. (b) Surface profiles along five different lines of nanotube cuts shown in (a).

concentric tubules with various degrees of chiralities (ranging from zigzag to armchair). Therefore, our MWNTs samples may possess zigzag, armchair, and chiral nanotubes and that would drive the catalytic particle along different directions on the surface of the CNT (not only along the tube axis). It is also important to consider the amount of defects present on the nanotube surface (vacancies, dopants, etc.) that could alter significantly the cuts on the tube surface. Regarding this issue, we should point out that both types of CNTs (MWNTs and  $\text{CN}_x$ MWNTs) exhibit a good degree of crystallinity under XRD analysis, being MWNTs the most crystalline (not shown here). For the case of  $\text{CN}_x$ MWNTs, nitrogen could be incorporated in the graphitic lattice and might affect considerably the straight cutting of the tubes. Theoretical simulations on graphene have predicted that defects within the graphitic planes could cause the nanoparticle to turn at a given angle (commonly  $60^\circ$  or  $120^\circ$ ).<sup>21,22</sup> Previous reports for  $\text{CN}_x$ MWNTs predict<sup>26</sup> that nitrogen bonded to the carbon atoms in a pyridinic way certainly induces voids in the graphitic layers, which could be the cause of more turns (e.g., random-like) during the cutting process.

It is also important to comment on the Fe particles used in the CVD nanotube growth, which remain encapsulated inside the nanotubes during the thermal cutting treatments. These Fe nanoparticles could also be exposed to the Ar–H atmosphere at high temperature ( $850^\circ\text{C}$ ). If so, the particle could become active and should also be capable of cutting the CNTs from the inside of the tubes, thus producing carbon nanoribbons and nanosheets.

As we have described in the Experimental Section, two different methods were used for depositing the catalytic particles on CNTs: (1)  $\text{CoCl}_2$  in EtOH impregnation and (2) Ni sputtering. According to the characterization performed, each method leads to different yields.

In the first method, the wetting of the CNT in the salt is important, because it is the source for the particle formation during the initial part of the experiment (1 h at  $500^\circ\text{C}$  in an Ar–H atmosphere). This method was used for very little amounts of nanotubes (10–30  $\mu\text{L}$  of the dispersed  $\text{CoCl}_2$ –CNT original solution). The Si wafers containing the CNT cut samples were dispersed ultrasonically but, since the wafer originally contained a very low amount of material,

the preparation of TEM grids was very challenging. According to the SEM, STEM, and TEM observations, we estimate that approximately 50% of the nanotubes have nucleated metal nanoparticles that resulted in the cutting of their walls (for the  $\text{CoCl}_2/\text{EtOH}$  concentration reported). Approximately 5% of the nanotubes in our samples were fully open longitudinally. We observed several hundred nanometers long cuts (up to  $1\ \mu\text{m}$ ). In addition, the depth of the cutting varies according to the size of the catalytic particle, and we estimated that approximately 20% of the cuts are deep enough to reach the hollow core of the nanotube. An important variable that can be fine-tuned is the concentration of  $\text{CoCl}_2$  in the original solution, since the amount and size of the nanoparticles nucleated in each nanotube could be increased by increasing that concentration. An excess of  $\text{CoCl}_2$  would have extreme results that could dissociate the whole carbon atoms from the tubes.

For the experiments performed using the sputter coater method, a relatively thick layer of carbon nanotubes was initially prepared. A thin layer of Ni was subsequently deposited on this film of CNTs using the magnetron sputtering. This method led to a much higher yield of CNT/cut-CNT material on the Si substrate after the cutting experiments. However, since only the superficial carbon nanotubes of the film were exposed to the Ni atoms, it is not possible to provide accurate numbers of the yields. Nevertheless, from the ultrasonic dispersion of the Si wafer we could easily transfer enough material to TEM grids, in order to perform further STEM and TEM observations.

From unzipped MWNTs we have demonstrated that pure carbon nanoribbons, partially open tubes, and nanosheets could be obtained. However, in  $\text{CN}_x\text{MWNTs}$  nitrogen is incorporated within the graphitic layers and further investigation needs to be performed in order to determine the role of nitrogen in the produced doped-ribbons. It has been predicted in the literature that doping agents (N or B) in graphene nanoribbons could induce remarkable modifications in the electronic and spin properties of such doped structures.<sup>28</sup> In comparison with recently reported methods for the production of GNRs from CNTs,<sup>17–19</sup> the present report constitutes a viable alternative route due to its simplicity and nonaggressive approach. The main thickness of our ribbons would roughly depend on the number of layers of the original CNT (ca. 20–50 layers in our case). Since the present process does not involve any aggressive chemical treatment, the resulting graphitic edges should be cleaner when compared to other methods reported in the literature. Finally, we envisage that these partially open carbon nanotubes could possess novel magnetoresistive properties.<sup>1</sup>

**Acknowledgment.** The authors are grateful to Y. I. Vega-Cantú, F. J. Rodríguez-Macías, G. Ramírez, F. Tristán, H. Martínez, S. Vega, and G. Pérez for their technical assistance. This work was supported in part by CONACYT-Mexico Grants: 58899-Inter American Collaboration (M.T.), 56787

(Laboratory for Nanoscience and Nanotechnology Research-LINAN), 48300 (E.M.S.), 45762 (H.T.), 45772 (M.T.), 2004-01-013/SALUD-CONACYT (M.T.), Fondo Mixto de San Luis Potosí 63001 S-3908 (M.T.), Fondo Mixto de San Luis Potosí 63072 S-3909 (H.T.), Postdoctoral Fellowship (A.L.E.), and PhD Scholarships (D.M.R., A.R.B.M., V.J.G.). The authors acknowledge the support from the Interconnect Focus Center, one of five research centers funded under the Focus Center Research Program, a Semiconductor Research Corporation program.

**Note Added after ASAP Publication.** This paper was published on the Web on August 19, 2009, with a figure citation error in the text. The corrected version was reposted on December 17, 2009.

**Supporting Information Available.** AFM images of two isolated pristine carbon nanotubes on a Si substrate, an unzipped  $\text{CN}_x\text{MWNT}$ , and pristine  $\text{CN}_x\text{MWNT}$ . This material is available free of charge via the Internet at <http://pubs.acs.org>.

## REFERENCES AND NOTES

- (1) Santos, H.; Chico, L.; Brey, L. Carbon nanoelectronics: unzipping tubes into graphene ribbons. arXiv:0904.3676v1 [cond-mat.mes-hall].
- (2) Novoselov, K. S.; Geim, A. K.; Morozov, S. V.; Jiang, D.; Zhang, Y.; Dubonos, S. V.; Grigorieva, I. V.; Firsov, A. A. *Science* **2004**, *306*, 666–669.
- (3) Li, X.; Wang, X.; Zhang, L.; Lee, S.; Dai, H. *Science* **2008**, *319*, 1229–1232.
- (4) Geim, A. K.; Novoselov, K. S. *Nat. Mater.* **2007**, *6*, 183–191.
- (5) Nakada, K.; Fujita, M.; Dresselhaus, G.; Dresselhaus, M. S. *Phys. Rev. B* **1996**, *54*, 17954.
- (6) Fujita, M.; Wakabayashi, K.; Nakada, K.; Kusakabe, K. *J. Phys. Soc. Jpn.* **1996**, *65*, 1920.
- (7) Yang, L.; Park, C. H.; Son, Y. W.; Cohen, M. L.; Louie, S. G. *Phys. Rev. Lett.* **2007**, *99*, 186801.
- (8) Son, Y. W.; Cohen, M. L.; Louie, S. G. *Nature* **2006**, *444*, 347.
- (9) Dalosto, S. D.; Levine, Z. H. *J. Phys. Chem. C* **2008**, *112*, 8196–8199.
- (10) Huang, B.; Li, Z. Y.; Liu, Z. R.; Zhou, G.; Hao, S. G.; Wu, J.; Gu, B. L.; Duan, W. H. *J. Phys. Chem. C* **2008**, *112*, 13442–13446.
- (11) Bets, K. V.; Yakobson, B. I. *Nano Res.* **2009**, *2*, 161–166.
- (12) Novoselov, K. S.; Geim, A. K.; Morozov, S. V.; Jiang, D.; Katsnelson, M. I.; Grigorieva, I. V.; Dubonos, S. V.; Firsov, A. A. *Nature* **2005**, *438*, 197–200.
- (13) Schedin, F.; Geim, A. K.; Morozov, S. V.; Hill, E. W.; Blake, P.; Katsnelson, M. I.; Novoselov, K. S. *Nat. Mater.* **2007**, *6*, 652–655.
- (14) Tapasztó, L.; Dobrik, G.; Lambin, P.; Biró, L. *Nat. Nanotechnol.* **2008**, *3*, 397–401.
- (15) Campos-Delgado, J.; Romo-Herrera, J. M.; Jia, X. T.; Cullen, D. A.; Muramatsu, H.; Kim, Y. A.; Hayashi, T.; Ren, Z. F.; Smith, D. J.; Okuno, Y.; Ohba, T.; Kanoh, H.; Kaneko, K.; Endo, M.; Terrones, H.; Dresselhaus, M. S.; Terrones, M. *Nano Lett.* **2008**, *8*, 2773–2778.
- (16) Terrones, M. *Nature* **2009**, *458*, 845–846.
- (17) Kosynkin, D. V.; Higginbotham, A. L.; Sinitskii, A.; Lomeda, J. R.; Dimiev, A.; Price, B. K.; Tour, J. M. *Nature* **2009**, *458*, 872–876.
- (18) Cano-Márquez, A. G.; Rodríguez-Macías, F. J.; Campos-Delgado, J.; Espinosa-González, C. G.; Tristán-López, F.; Ramírez-González, D.; Cullen, D. A.; Smith, D. J.; Terrones, M.; Vega-Cantú, Y. I. *Nano Lett.* **2009**, *9*, 1527–1533.
- (19) Jiao, L.; Zhang, L.; Wang, X.; Diankov, G.; Dai, H. *Nature* **2009**, *458*, 877–880.
- (20) Datta, S. S.; Strachan, D. R.; Khamis, S. M.; Johnson, A. T. C. *Nano Lett.* **2008**, *8*, 1912–1915.

- (21) Ci, L.; Xu, Z.; Wang, L.; Gao, W.; Ding, F.; Kelly, K. F.; Yakobson, B. I.; Ajayan, P. M. *Nano Res.* **2008**, *1*, 116.
- (22) Ci, L.; Song, L.; Jariwala, D.; Gao, W.; Elias, A. L.; Terrones, M.; Ajayan, P. M. *Adv. Mater.*, in press.
- (23) Baker, R. T. K.; Sherwood, R. D.; Derouane, E. G. *J. Catal.* **1982**, *75*, 382–395.
- (24) Pinault, M.; Mayne-L’Hermite, H.; Reynaud, C.; Beysac, O.; Rouzaud, J. N.; Clinard, C. *Diamond Relat. Mater.* **2004**, *13*, 1266–1269.
- (25) Botello-Méndez, A.; Campos-Delgado, J.; Morelos-Gómez, A.; Romo-Herrera, J. M.; Rodríguez, A. G.; Navarro, H.; Vidal, M. A.; Terrones, H.; Terrones, M. *Chem. Phys. Lett.* **2008**, *453*, 55–61.
- (26) Terrones, M.; Kamalakaran, R.; Seeger, T.; Rühle, M. *Chem. Commun.* **2000**, *23*, 2335–2336.
- (27) Liu, M.; Cowley, J. M. *Carbon* **1995**, *33* (2), 225–232.
- (28) Cervantes-Sodi, F.; Csányi, G.; Piscanec, S.; Ferrari, A. C. *Phys. Rev. B* **2008**, *77*, 165427.